$Zr_{55}Al_{10}Ni_5Cu_{30}$非晶钎料熔体与 α-$Al_2O_3$ 和 ZrO_2 陶瓷的润湿性

郑小红，　沈　平
（吉林大学 汽车材料教育部重点实验室，长春　130025）

郑小红

摘　要：利用改良座滴法研究了 $Zr_{55}Al_{10}Ni_5Cu_{30}$ 非晶钎料熔体与多晶 α-Al_2O_3 和 ZrO_2 陶瓷的润湿行为和界面特征．结果表明，$Zr_{55}Al_{10}Ni_5Cu_{30}$/α-$Al_2O_3$ 体系具有极好的润湿性，在 1 133～1 193 K 温度范围内平衡接触角均为 0°．$Zr_{55}Al_{10}Ni_5Cu_{30}$/$ZrO_2$ 之间的润湿性较差，但在 1 133～1 253 K 温度范围内随着时间的延长，润湿性逐渐得到改善．两个体系均存在一定程度的界面反应．润湿动力学和界面显微结构的研究表明液滴合金中的活性元素（如 Zr）在界面尤其是三相线前沿的吸附和堆积速度对润湿起了决定性的作用，而界面反应的贡献则相对较小．

关键词：非晶钎料；润湿性；界面反应；吸附
中图分类号：TG425　　文献标识码：A　　文章编号：0253－360X(2009)11－0057－04

0　序　　言

活性钎焊以其工艺简单、连接强度高、成本相对低等一系列优点而成为金属/陶瓷连接的首选技术．近些年来，随着非晶合金的快速发展，非晶钎料已经成为金属/陶瓷或陶瓷/陶瓷钎焊领域的一个重要研究方向．国内外许多学者均开展了这方面的研究[1－3]．结果表明，使用非晶钎料能比晶态钎料在更低的温度、更短的时间内实现连接，而且可以获得比晶态钎料更好的接头性能．尤其是由具有良好非晶形成能力和活性 Ti，Zr 元素组成的铜基或锆基非晶钎料有望取代目前应用广泛但较昂贵的 Ag-Cu-Ti 钎料，并可望用于更高温的场合．

众所周知，在采用钎焊或瞬态液相连接方法实现钎料与其它材料的连接过程中，润湿性起着十分重要的作用．但是，到目前为止国内外关于非晶合金与陶瓷润湿性的研究还十分有限[4－7]．文中利用改良座滴法研究了 $Zr_{55}Al_{10}Ni_5Cu_{30}$ 非晶合金熔体与多晶 α-Al_2O_3 和 ZrO_2 陶瓷的润湿性、反应特征和界面结构，其目的是为开发新型的锆基非晶合金钎料，并且为实现钎料与 α-Al_2O_3 和 ZrO_2 的连接提供指导．

收稿日期：2009－06－02
基金项目：新世纪优秀人才支持计划项目（NCET－07－0360）

1　试验方法

试验所用的 $Zr_{55}Al_{10}Ni_5Cu_{30}$ 非晶合金是利用高纯 Zr99．8，Al99．99，　Ni99．98，Cu，99．999（质量分数，%）在钛吸氧的高纯 99．999%Ar 气氛下通过 4 次电弧熔炼然后吸铸到 φ7 mm 的铜模中得到．吸铸后的试样经 X 一射线衍射（XRD）分析表明完全为非晶相．关于制备细节详见文献[7]．为了获得准确的接触角，将非晶合金棒用金刚石切割机切成小立方体形状，并且保证每个小立方体的质量在 30 mg ± 5 mg．在润湿试验之前将非晶合金置于丙酮中用超声波清洗 3 遍以去除表面污渍．

试验中所用的基板是纯度为 99．9%的多晶 α-Al_2O_3 和 ZrO_2（摩尔分数为 97% ZrO_2-3% Y_2O_3）基片，尺寸均为 20 mm × 20 mm × 5 mm．表面经过 20，10，5，0．5 μm 的金刚石研磨膏抛光．利用 DEKTAK 6M 台阶仪以 100 μm/s 的速度在 2 mm 的范围内测定基板表面的平均粗糙度（Ra）分别为 100，16 nm．基板抛光后同样置于丙酮中超声波清洗 3 遍以备用．

利用改良座滴法在真空气氛下分别测定不同温度下 $Zr_{55}Al_{10}Ni_5Cu_{30}$ 非晶合金熔体在 α-Al_2O_3 和 ZrO_2 基板上的润湿行为．试验装置和具体的试验步骤如文献[7]所述．试验时先在室温下抽真空至 5×10^{-4}

Pa，然后以 20 K/min 的速度升温至 1 473 K，保温 10 min，再以 15 K/min 的速度降到试验温度，此时真空度约为 2×10^{-4} Pa．待温度稳定(±1 K)以后，将 $Zr_{55}Al_{10}Ni_5Cu_{30}$ 非晶合金从真空室外掉落至陶瓷基板上．同时用高分辨率(1 504×1 000 dpi)相机以最快 2 张/s 的速度拍照．

润湿试验之后试样以 20 K/min 的速度随炉冷却．利用轴对称液滴形状分析(ADSA)软件对拍摄的照片进行处理，获得接触角随时间变化的曲线图．对部分试样进行冷镶嵌，并从试样中心沿纵截面切开，研磨并抛光。利用配有能谱仪(EDS)的扫描电镜(SEM)和场发射扫描电镜(FESEM)观察试样的界面结构．采用选择性腐蚀技术去除凝固的液滴以露出界面区域．利用 FESEM 观察暴露的固—液—气三相交汇处和界面的显微结构，并利用微区 XRD(束斑直径为 800 μm)对界面物相进行检测．

2 试验结果与分析

2.1 润湿行为

图 1 为不同温度下 $Zr_{55}Al_{10}Ni_5Cu_{30}$ 非晶合金熔体在 Al_2O_3 和 ZrO_2 基板上的接触角随时间变化曲线．从图 1a 中可知，在 1 133～1 193 K 温度的范围内，$Zr_{55}Al_{10}Ni_5Cu_{30}$ 非晶合金熔体在 Al_2O_3 基板上的起始接触角在 83°～88°之间．接触角在最初的几分钟内快速减小然后渐趋 0°，表明该体系具有极好的润湿性．从图 1b 中可见，在 1 133～1 253 K 温度范围内 $Zr_{55}Al_{10}Ni_5Cu_{30}$ 非晶合金熔体在 ZrO_2 基板上的起始接触角在 115°～102°之间，然后随时间的延长慢慢减小．最终接触角分别为 53°，59°，63°和 78°．与一般体系不同的是此体系的起始接触角随着温度的升高逐渐减小，最终接触角却随温度的升高逐渐增大，即润湿性表现出反常的温度依赖性．

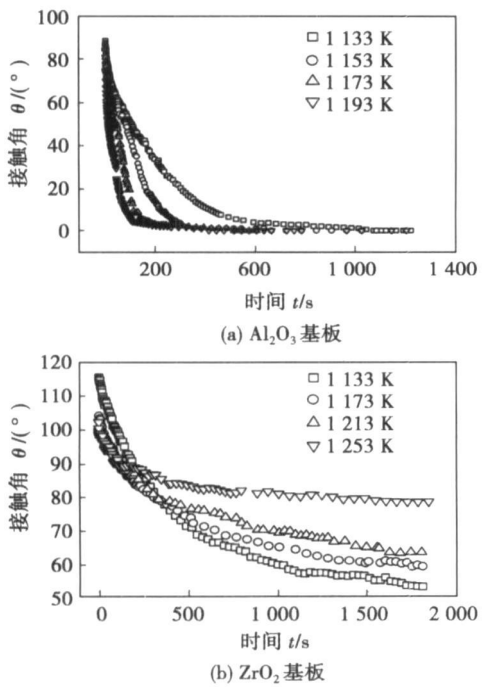

图 1 非晶合金熔体在不同基板上的接触角随时间变化曲线

Fig. 1 Variations in contact angle with time for molten $Zr_{55}Cu_{30}Al_{10}Ni_5$ alloy on different surfaces

2.2 界面形貌与界面反应

图 2a 为 $Zr_{55}Al_{10}Ni_5Cu_{30}$ 非晶熔体在 Al_2O_3 基板上 1 173 K 保温 20 min 后随炉冷却的界面显微组织形貌，从图中可见存在一薄层较为连续的反应层．图 2b 为凝固液滴在盐酸溶液中腐蚀后三相交汇处的显微组织形貌．图 3 为 $Zr_{55}Al_{10}Ni_5Cu_{30}$ 非晶合金熔体在 Al_2O_3 基板上冷却后试样不同位置的 XRD 衍射图。结合图 3a 的 XRD 微区分析结果可知反应产物为 ZrO_2．反应式为

$$3[Zr]+2Al_2O_3=4[Al]+3ZrO_2 \quad (1)$$

在 1 173 K 时该反应的标准吉布斯自由能变化 ΔG^0 为 −20.93 kJ/mol[8]．因此反应在热力学上是可行的．

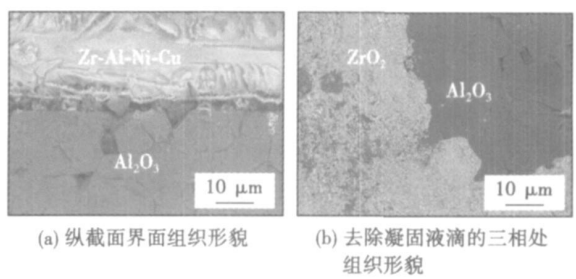

图 2 非晶熔体在 Al_2O_3 基板上的界面显微形貌

Fig. 2 Microstructure of $Zr_{55}Al_{10}Ni_5Cu_{30}/Al_2O_3$ sample

在 $Zr_{55}Al_{10}Ni_5Cu_{30}/Al_2O_3$ 体系的三相线前沿发现了宽度约为 1.5～2 mm，厚为 2～6 μm 的前驱膜．在金属—陶瓷体系中形成前驱膜往往意味着好的润湿性[9]．XRD 微区分析(图 3b)并结合 EDS 能谱分析表明，前驱膜的主要成分是 Zr 和 Cu 元素．然而经典的蒸发—冷凝理论及表面扩散理论均无法解释这里出现的前驱膜．只有用 Xian[9] 提出的快速吸附并形成薄膜流动的模型才可以解释，这一点在文献[7]中有详细的阐述．

图 4 给出了 $Zr_{55}Al_{10}Ni_5Cu_{30}$ 非晶合金熔体在 ZrO_2 基板上 1 253 K 保温 30 min 后随炉冷却的界面显微组织形貌．在界面处发现一层连续的反应层，结合

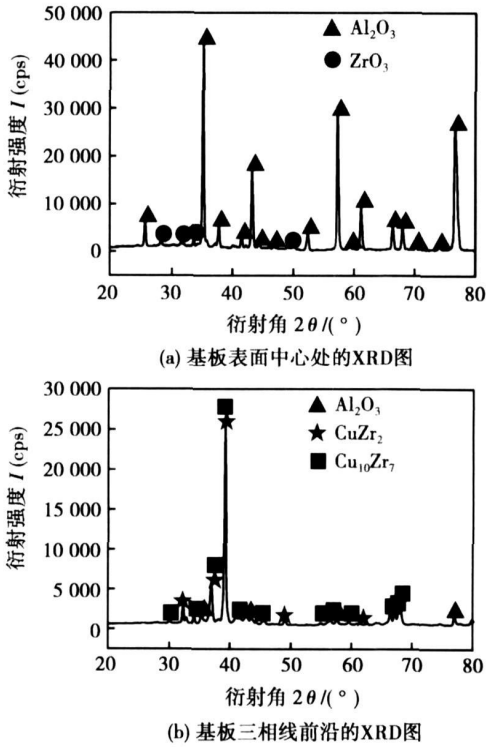

图 3　Al_2O_3 体系试样不同位置的 XRD 图

Fig. 3　X-ray patterns for phases at different locations of wetting sample

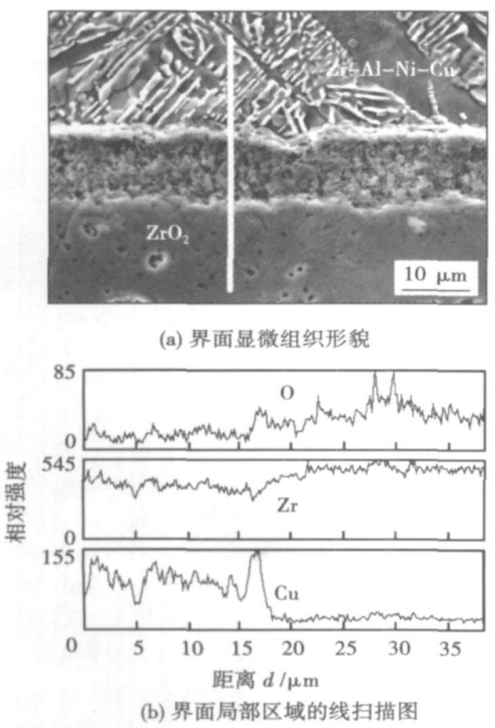

图 4　非晶熔体在 ZrO_2 基板上的界面组织形貌

Fig. 4　Microstructure of $Zr_{55}Al_{10}Ni_5Cu_{30}/ZrO_2$ sample

EDS 线扫描分析图可知，在反应层处 Zr 元素含量存在梯度，说明界面反应层处的锆含量与 ZrO_2 基板中的锆含量并不相同．由此可见锆与 ZrO_2 发生了如下反应，即

$$(2-x)ZrO_2 + xZr = 2ZrO_{2-x} \qquad (2)$$

Durov 等人[10]在 Cu-Ga-Zr 合金与 ZrO_2 的润湿性研究中也观察到界面处形成了非计量比的 ZrO_{2-x}．

2.3　润湿机理

由以上的分析可知，$Zr_{55}Al_{10}Ni_5Cu_{30}/Al_2O_3$ 和 $Zr_{55}Al_{10}Ni_5Cu_{30}/ZrO_2$ 体系均属于反应润湿体系．国际上关于反应润湿体系的润湿驱动力及界面反应的作用长期以来一直存在很大的争议．为了确定吸附和界面反应对 $Zr_{55}Al_{10}Ni_5Cu_{30}/Al_2O_3$ 体系润湿性的相对贡献，作者进行了在 1 173 K 保温 150 s 后切断电源快速冷却的试验．在 150 s 时试样的接触角为 12°．图 5 为去除凝固液滴后三相交汇处的界面显微组织形貌，在界面处并没有明显而连续的反应产物．此外，在 1 173 K 时 $Zr_{55}Al_{10}Ni_5Cu_{30}/ZrO_2$ 体系的起始接触角为 108°±5°，保温 30 min 后接触角减小到 59°±1°．因此，初步认为在研究中锆的吸附以及随后在三相线前沿形成的 Zr-Cu 前驱膜而非界面反应是促成在 Al_2O_3 基板上完全润湿的主要原因．

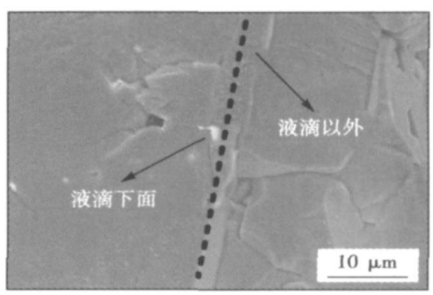

图 5　$Zr_{55}Al_{10}Ni_5Cu_{30}/Al_2O_3$ 的界面形貌

Fig. 5　Microstructure of $Zr_{55}Al_{10}Ni_5Cu_{30}/Al_2O_3$ sample

图 6 为 1 133 K 时 $Zr_{55}Al_{10}Ni_5Cu_{30}$ 非晶合金熔体在 ZrO_2 基板上保温 30 min 的界面显微组织形貌和元素面扫描图．结合 EDS 能谱分析可知，三相线前沿吸附了大量的锆。由于铜与锆具有较强的亲和力，铜随着锆而移动，所以在三相线前沿也堆积了较多的铜．图 7 为 1 253 K 时 $Zr_{55}Al_{10}Ni_5Cu_{30}$ 非晶合金熔体在 ZrO_2 基板上保温 30 min 的界面显微组织形貌和元素面扫描图．结合 EDS 能谱分析可知，三相线前沿与反应层基本持平，Zr-Cu 吸附层并没有跨越三相线而形成显著的前驱膜．

由于润湿在很大程度上取决于三相线的组态，

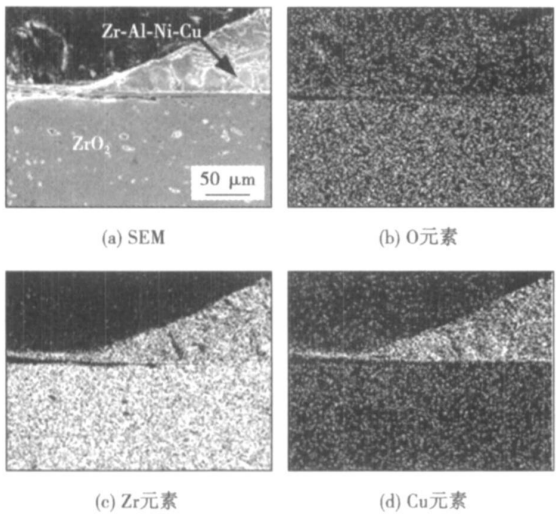

图 6 1 133 K 温度下 ZrO_2 体系的组织形貌和元素面扫描图

Fig. 6 Microstructures of $Zr_{55}Al_{10}Ni_5Cu_{30}/ZrO_2$ samples at 1 133 K

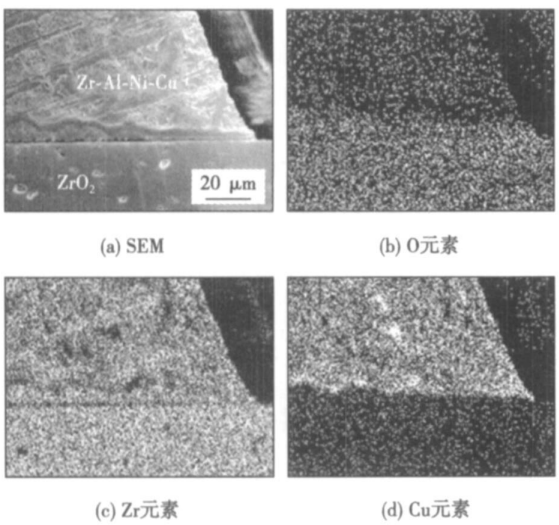

图 7 1 253 K 温度下 ZrO_2 体系的组织形貌和元素面扫描图

Fig. 7 Microstructures of $Zr_{55}Al_{10}Ni_5Cu_{30}/ZrO_2$ samples at 1 253 K

由此可以解释 $Zr_{55}Al_{10}Ni_5Cu_{30}/ZrO_2$ 体系这种异常的润湿与温度依赖性的特征. 在较低温度(1 133 K)时,活性元素Zr移动到界面尤其是三相交汇处的速度比界面反应消耗锆的速度要快,导致锆在界面的吸附堆积,并移动到三相线前沿. 这种吸附降低了固液界面能. 最重要的是,锆在三相线前沿的堆积使得后续的铺展相当于是在一种已经润湿的表面上进行,从而导致接触角的迅速降低。随着温度的升高,铺展速度变慢. 这是因为反应速度随着温度升高而增大,导致锆吸附到界面上的速度可能赶不上由于界面反应所消耗的速度,从而在界面形成了较显著的反应产物层,界面反应产物的控制作用逐渐加强. 但是从接触角的变化幅度来看,相比于吸附引起的前驱膜效应,界面反应产物对该体系润湿性的改善作用依然较小.

综上所述,活性元素Zr在界面尤其是三相线前沿的吸附和堆积对于 $Zr_{55}Al_{10}Ni_5Cu_{30}/\alpha\text{-}Al_2O_3$ 和 $Zr_{55}Al_{10}Ni_5Cu_{30}/ZrO_2$ 体系的润湿都起到了决定性的促进作用,而界面反应的作用相对较小.

3 结 论

(1) $Zr_{55}Al_{10}Ni_5Cu_{30}/\alpha\text{-}Al_2O_3$ 体系具有极好的润湿性. 在1 133 ~1 193 K温度范围内的起始接触角在83°~88°之间,平衡接触角均为0°,铺展速度很快. $Zr_{55}Al_{10}Ni_5Cu_{30}/ZrO_2$ 体系的润湿性较差,在1 133 ~1 253 K时的起始接触角在115°~102°之间. 随着时间的延长接触角变小,但最终接触角随着温度的升高反而增大.

(2) $Zr_{55}Al_{10}Ni_5Cu_{30}/\alpha\text{-}Al_2O_3$ 和 $Zr_{55}Al_{10}Ni_5Cu_{30}/ZrO_2$ 体系均存在界面反应. 反应产物分别为 ZrO_2 和非计量比的 ZrO_{2-x}.

(3) 液滴合金中的活性元素Zr在界面尤其是三相线前沿的吸附和堆积速度对以上两个体系的润湿起了决定性的作用,界面反应的作用则相对较小.

参考文献:

[1] 熊华平. CuNiTiB急冷钎料对 Si_3N_4 陶瓷的连接[J]. 中国有色金属学报, 1999, 9(4): 764—768.
Xiong Huaping. Joining of Si_3N_4 to Si_3N_4 using rapidly-solidified Cu-NiTiB brazing filler foils[J]. The Chinese Journal of Nonferrous Metals, 1999, 9(4): 764—768.

[2] 邹家生, 许志荣, 蒋志国, 等. Ti-Zr-Ni-Cu 非晶钎料[J]. 焊接学报, 2005, 26(10): 51—53.
Zou Jiasheng, Xu Zhirong, Jiang Zhiguo, *et al*. Ti-Zr-Ni-Cu amorphous welding materials[J]. Transactions of the Chian Welding Institution, 2005, 26(10): 51—53.

[3] Naka M, Tanaka T, Okamoto I. Joining of silicon nitride using amorphous Cu-Ti filler metal[J]. Transactions of JWRI, 1987, 16(1): 83—90.

[4] Schroers J, Samwer K, Szuecs F, *et al*. Characterization of the interface between the bulk glass forming alloy $Zr_{41}Ti_{14}Cu_{12}Ni_{10}Be_{23}$ with pure metals and ceramics[J]. Journal of Materials Research, 2000, 15(7): 1617—1621.

[5] Xu Q G, Zhang H F, Hu Z Q. Wetting behavior of $Zr_{55}Cu_{30}Al_{10}Ni_5$ melt on alumina[J]. The Chinese Journal of Nonferrous Metals, 2005, 15(1): 45—50.

[下转第 64 页]

变形，β-$Mg_{17}(Al, Zn)_{12}$ 相的脆性导致裂纹很容易形成与扩展，同时 β-$Mg_{17}(Al, Zn)_{12}$ 相与 α-Mg 基体在界面处由于受到外力作用时易产生应力集中，在应力集中的作用下，使得硬脆 β-$Mg_{17}(Al, Zn)_{12}$ 相沿 α-Mg 界面被拉开而产生裂纹，从而导致接头拉伸断口表现为较明显的沿晶脆性断裂特性.

3 结 论

(1) 以 Al-Mg-Zn 钎料在氩气保护条件下可以实现对变形镁合金 AZ31B 的高频感应钎焊.

(2) 钎缝中钎料与母材发生溶解与扩散反应生成离异共晶组织 α-Mg + β-$Mg_{17}(Al, Zn)_{12}$，主要生成相为 α-Mg 相和 β-$Mg_{17}(Al, Zn)_{12}$ 相. 钎焊对接接头平均抗拉强度为 45 MPa，搭接接头平均抗剪强度为 27 MPa.

(3) 钎焊对接和搭接接头的拉伸断口均表现为较明显的沿晶脆性断裂特性，断裂主要产生在沿 α-Mg 晶界网状分布的粗大 β-$Mg_{17}(Al, Zn)_{12}$ 硬脆相处.

参考文献：

[1] Shapiro A E. Brazing magnesium alloys and magnesium matrix composites[J]. Welding Journal, 2005, 84(10): 33—43.

[2] Committee on brazing and soldering. Brazing manual[M]. Miami: American Welding Society, 1975.

[3] Cand I, Arne S M. Entwicklung von magnesium basis legierungen zum loten von leichtmetallen[D]. Aachen: Rheinisch Westfälische Technische Hochschule Aachen, 2005.

[4] Watanabe T, Komatu S, Yanagisawa A, *et al*. Development of flux and filler metal for brazing magnesium alloy AZ31B[J]. Yosetsu Gakkai Ronbunshu/Quarterly Journal of the Japan Welding Society, 2004, 22(1): 163—167.

[5] Watanabe T, Komatu S, Oohara K. Development of flux and filler metal for brazing magnesium alloy AZ31B[J]. Welding Journal, 2005, 84(3): 37—40.

[6] Baker H. Alloy phase diagrams[M]. Ohio: Materials Park, 2006.

[7] Li Y, Terence G, Langdon. Creep behavior of an AZ91 magnesium alloy reinforced with alumina fibers[J]. Metallurgical and Materials Transactions A, 1999, 30(8): 2059—2066.

[8] Liu L M, Zhang Z D, Song G. Mechanism and microstructure of oxide fluxes for gas tungsten arc welding of magnesium alloy[J]. Metallurgical and Materials Transactions A, 2007, 38(3): 649—658.

[9] Czerwinski F, Zielinska L A, Pinet P J, *et al*. Correlating the microstructure and tensil properties of a thixomolded AZ91D magnesium[J]. Acta Materialia, 2001, 49(7): 1225—1235.

作者简介：马 力，男，1971 年出生，博士研究生. 主要从事镁合金钎焊材料及钎焊工艺研究. 发表论文 2 篇.

Email：mali2050@emails.bjut.edu.cn

[上接第 60 页]

[6] Xu Q G, Wu B L, Zhang H F, *et al*. Wettability of molten $Zr_{55}Cu_{30}Al_{10}Ni_5$ on alumina and zirconia[J]. Rare Metals, 2007, 26(3): 213—217.

[7] Shen P, Zheng X H, Lin Q L, *et al*. Wetting of polycrystalline α-Al_2O_3 by molten $Zr_{55}Cu_{30}Al_{10}Ni_5$ metallic glass alloy[J]. Metallurgical and Materials Transactions A, 2009, 40A: 444—449.

[8] Chase M W, Davies C A, Downey J R, *et al*. JANAF thermochemical tables[J]. Journal of Physical Chemistry Reference Data, 1985, 14(1): 156, 1691.

[9] Xian A P. Precursor film of tin-based active solder wetting on ceramics[J]. Journal of Materials Science, 1993, 28(4): 1019—1030.

[10] Durov A V, Naidich Y V, Kostyuk B D. Investigation of interaction of metal melts and zirconia[J]. Journal of Materials Science, 2005, 40(9—10): 2173—2178.

作者简介：郑小红，女，1976 年出生，博士研究生. 主要研究方向为材料界面形成与控制. 发表论文 12 篇.

Email：xhzheng1976@126.com

shaped and the thickness of IMC is much thinner when SAC0307 solder added 0.05% Ni is used. The consumption of Ni layer is nearly the same using both solders after the first time reflow soldering, but the residual thickness of the Ni layer in SAC0307/Ni solder is thinner than that in SAC0307-0.05Ni/Ni after aging for 384 h. So solders with a little Ni element can decrease the consumption rate of Ni layer effectively during aging, that is, the aging-resistant ability of Ni pad is improved obviously.

Key words: SAC0307-*x*Ni; solder; Ni substrate; IMC; aging

Wettability of molten $Zr_{55}Al_{10}Ni_5Cu_{30}$ metallic glass brazing alloy on α-Al_2O_3 and ZrO_2 ZHENG Xiaohong, SHEN Ping (Key Laboratory of Automobile Materials Ministry of Education, Jilin University, Changchun 130025, China). p 57—60, 64

Abstract: The wettability and interfacial characteristics of molten $Zr_{55}Al_{10}Ni_5Cu_{30}$ metallic glass brazing alloy on polycrystalline α-Al_2O_3 and ZrO_2 substrates were studied using a modified sessile drop method. The results show that the wettability of the $Zr_{55}Al_{10}Ni_5Cu_{30}$/$\alpha$-$Al_2O_3$ system is excellent with the final contact angles approaching zero degree at 1 133-1 193 K. However, the wettability of the $Zr_{55}Al_{10}Ni_5Cu_{30}$/$ZrO_2$ system is poor, but it can be progressively improved with the elapse of time during the isothermal dwelling in the temperature range of 1 133-1 253 K. A certain extent of interfacial reaction happens in both systems. The investigation on the spreading kinetics and interfacial microstructure indicates that the adsorption of the active atoms such as Zr at the interface, particularly at the triple junctions, plays a key role in determining the wettability, whereas the contribution of the interfacial reaction is relatively minor.

Key words: Metallic glass brazing alloy; wettability; interfacial reaction; adsorption

Microstructure and mechanical properties of magnesium alloy AZ31B joint brazed with Al-Mg-Zn filler metal MA Li[1], HE Dingyong[1], LI Xiaoyan[1], JIANG Jianmin[1], WANG Lizhi[2] (1. College of Materials Science and Engineering, Beijing University of Technology, Beijing 100124, China; 2. Welding Research Institute of Central Research Institute of Building & Construction, China Metallurgical Group Corporation, Beijing 100088, China). p 61—64

Abstract: High-frequency induction brazing of wrought magnesium alloy AZ31B with Al-Mg-Zn filler metal was investigated. Microscopic structure, the phases and the mechanical properties of brazed joint were studied. The microstructure and formation phases at the interface in the brazed joint were investigated by scanning electron microscopy (SEM), X-ray diffraction instrument (XRD) and energy dispersive spectrometer (EDS). The strength of the brazed joint and the microhardness of the formation phases were also tested. The results show that, Al-Mg-Zn filler metal reacting with the base metal AZ31B, and α-Mg+β-$Mg_{17}(Al, Zn)_{12}$ divorced eutectic structure is formed in the brazed joint. Microhardness of the base metal AZ31B is the smallest and β-$Mg_{17}(Al, Zn)_{12}$ phase of the brazed joint is the hardest. Both the butt joint and the overlap joint exhibit intergranular fracture mode, the fracture comes from hard brittle phase β-$Mg_{17}(Al, Zn)_{12}$ of α-Mg+β-Mg17$(Al, Zn)_{12}$ divorced eutectic structure.

Key words: AZ31B magnesium alloy; Al-Mg-Zn filler metal; brazing; divorced eutectic; joint strength

Failure of soldered joint during thermal fatigue test LIN Jian[1], LEI Yongping[1], ZHAO Haiyan[2], WU Zhongwei[1] (1. College of Materials Science and Engineering, Beijing University of Technology, Beijing 100124, China; 2. Department of Mechanical Engineering, Tsinghua University, Beijing 100084, China). p 65—68, 72

Abstract: The failure process of soldered joint in SMT was investigated by electrical resistance measurement method and crack observation method. The characteristics of electrical resistance value variation of lead-tin and lead-free soldered (SAC305) joints during the thermal fatigue test were obtained. And at the same time the crack propagation in soldered joint was observed. According to these measurements, the failure rules of lead-tin and lead-free soldered joint were compared. The relationship between electrical resistance value variation and crack propagation of soldered joint during thermal fatigue test was studied by FEM, and an empirical criterion to estimate the failure of the soldered joint in the thermal fatigue test was obtained based on electrical resistance value variation. The experimental results show that the lead-free soldered joint has a higher resistibility in thermal fatigue than the traditional lead-tin soldered joint. The criterion based on electrical resistance value variation was founded from the experimental and simulation results.

Key words: SMT; soldered joint; thermal fatigue; electrical resistance; crack

TiN/Ti composite coating deposited on titanium alloy substrate by reactive electric-spark HAO Jianjun[1,2], PENG Haibin[1], HUANG Jihua[3], MA Yuejin[1], LI Jianchang[1] (1. College of Electromechanical Engineering, Agriculture University of Hebei, Baoding 071001, Hebei, China; 2. Light Metal Materials Engineering Research Center of Hebei, Baoding 071000, Hebei, China; 3. School of Materials Science and Engineering, University of Science and Technology of Beijing, Beijing 100083, China). p 69—72

Abstract: TiN/Ti composite coating was deposited on TC4 titanium alloy substrate with the self-made special gas-filled-closed electric-spark deposition device and electric-spark deposition machine modeled DZ-1400, the industry pure titanium (TA2) was used as electrode and the industry pure nitrogen gas as shielding and reacting atmosphere. The microstructures, interfacial behavior, phase and element in the coatings were investigated by scanning electronic microscope, X-ray diffraction and X-ray photo spectrum. The microhardness of coatings was tested and its wear-resistance property was tested by the self-made abrasion machine and compared with W18Cr4V rapid steel treated by quenching. The results show that an excellent bonding between the coating and substrate is ensured by the strong metallurgical interface. The coatings are mainly composed of Ti and synthesized TiN. The highest microhardness of coating reaches to 1 388 HV0.1, which is six times higher than that of the substrates. Wear resistance of the coatings is excellent.

Key words: reactive electric-spark deposition; TiN; composite coating; titanium alloy

Influence of transverse alternative magnetic field frequency on microstructure and properties of plasma arc surfacing layer LIU Zhengjun, ZHAO Qian, CI Honggang, SU Yunhai (School of